EDGE ARTICLE

Towards the object-oriented design of active hydrogen evolution catalysts on single-atom alloys†

Chuan Zhou, [a] Jia Yue Zhao,[b] Peng Fei Liu,[b] Jianfu Chen,[a] Sheng Dai,[c] Hua Gui Yang,[b] P. Hu[ad] and Haifeng Wang *[a]

Given a desired property, locating relevant materials is always highly desired but very challenging in a range of areas, including heterogeneous catalysis. Obviously, object-oriented design/screening is an ideal solution to this problem. Herein, we develop an inverse catalyst design workflow in Python (CATIDPy) that utilizes a genetic-algorithm-based global optimization method to guide on-the-fly density functional theory calculations, successfully realizing the highly accelerated location of active single-atom alloy (SAA) catalysts for the hydrogen evolution reaction (HER). 70 binary and 752 ternary SAA candidate catalysts are identified for the HER. Furthermore, *via* considering the segregation stability and cost of materials, we extracted 6 binary and 142 ternary SAA candidate catalysts that are recommended for experimental synthesis. Remarkably, guided by these theoretical identifications, homogeneously dispersed Ni-based bimetallic catalysts (*e.g.*, NiMo, NiAl, Ni$_3$Al, NiGa, and NiIn) were synthesized experimentally to test the reliability of the CATIDPy workflow, and they showed superior HER performance to bare Ni foam, indicating huge potential for use in real-world water electrolysis techniques. Perhaps more importantly, these results demonstrate the capacity of such a proposed approach for investigating unexplored chemical spaces to efficiently design promising catalysts without knowledge from the expert domain, which has far-reaching implications.

Introduction

The rapid development of density functional theory (DFT) has led to an unprecedented atomic-scale understanding of catalytic processes and catalyst screening in recent decades. Currently, a rational catalyst design strategy usually consists of two subtasks: one is the development of a descriptor-based approach[1–3] for reducing the dimensionality of the parameter space to a few descriptors (preferably 1–2 adsorption energies) using so-called scaling relations and Brønsted–Evans–Polanyi relations,[4–8] which illustrate the relation between these descriptors and activity, resulting in volcano plots.[8,9] The other

one still remains, however, a grand challenge: finding the specific materials meeting the requirement of the activity descriptor. Currently, the approaches to achieve this target include: searching databases,[10–20] identifying the structure–reactivity relationship[21–24] and machine learning methods.[25–27] Thereinto, (i) database construction requires a lot of early effort and is not friendly to the unexplored catalytic systems; (ii) the establishment of structure–reactivity relationship is inseparable from the support of experts' domain knowledge; (iii) although machine learning methods have attracted extensive attention, much effort is usually needed for the feature extraction with expert knowledge and training the model still requires a certain amount of pre-processing data. Essentially, searching a target material can be regarded as a discrete optimization problem in the tremendous material/configuration space; meanwhile, the inherently catalytic information could be automatically learned by an optimization algorithm. Therefore, developing an automated, efficient and oriented catalyst screening strategy is extremely desirable, and should constitute a basis for achieving a rational catalyst design.

Exploring clean and renewable energy sources is currently an urgent issue due to the ascending consumption of fossil fuels and environmental contamination.[28,29] Water splitting, especially the hydrogen evolution reaction (HER),[25,30–34] is one of the most promising reactions in electrochemistry and the simplest

[a]Key Laboratory for Advanced Materials, Centre for Computational Chemistry, Research Institute of Industrial Catalysis, East China University of Science and Technology, Shanghai, 200237, China. E-mail: hfwang@ecust.edu.cn

[b]Key Laboratory for Ultrafine Materials of Ministry of Education, Shanghai Engineering Research Center of Hierarchical Nanomaterials, East China University of Science and Technology, Shanghai, 200237, China

[c]Key Laboratory for Advanced Materials, Feringa Nobel Prize Scientist Joint Research Center, Institute of Fine Chemicals, East China University of Science and Technology, Shanghai, 200237, China

[d]School of Chemistry and Chemical Engineering, The Queen's University of Belfast, Belfast BT9 5AG, UK

† Electronic supplementary information (ESI) available. See DOI: 10.1039/d1sc01018b

way to produce hydrogen efficiently and in an environment-friendly manner. Generally, Pt-based electrocatalysts with a highly catalytic activity are recognized as superior HER catalysts in acid media to achieve favorable reaction kinetics.[35–39] However, their scarcity, as well as high cost, limit their industrial-scale applications. While in alkaline media, the Ni–Mo alloy is universally acknowledged as a highly active HER catalyst due to its similar surface electronic state to that of platinum.[40–43] Nevertheless, designing cheaper, stable and active HER catalysts has been one of the main goals in the field of renewable energy research.

Single-atom alloys (SAAs)[44–48] are a class of single-atom catalysts in which an atomically active metal is generally dispersed in a less-active metal host, resulting in well-defined local coordination environments of active sites and unique catalytic properties from the individual components.[49–56] Currently, a number of studies focusing on SAA catalysts are reported in this field. For example, Li et al.[57] identified Cu–Pt dual sites on Pd nanorings, exhibiting a high catalytic activity for HERs. Du et al.[58] synthesized a RuAu SAA using laser ablation in liquid, which gives a high stability and a low overpotential for the HER in alkaline media. Sautet and co-workers[59] showed single-nickel-atom-modified Pt nanowires with an enhanced activity towards HERs. Despite the progress, reports on the rational design of highly active SAA catalysts for HERs are rare. Perhaps more importantly, an efficient and automatic approach to achieve this aim is still lacking. One conceivable reason is that the sample search space is too large to be explored exhaustively and expert knowledge of the structure–composition activity remains far from sufficient. For instance, considering the situation of one site of one specific surface of ternary SAAs (consisting of one host metal and two guest metals), the search space could form 8000 possibilities with a combination of 20 different elements, resulting in a great obstacle in rationally screening high-performance catalysts by resorting to DFT calculations.

To this end, in this work a Python-based software for the inverse design of high-performance catalyst (namely CATIDPy) is developed, which enables an automated and object-oriented search, instructing the on-the-fly DFT calculations by virtue of a genetic-algorithm-based (GA) global optimization method. By taking the SAA-catalyzed HER system as a case study, we efficiently screen out 70 binary and 752 ternary SAA catalysts superior for HERs without expert domain knowledge and a portion of these were verified experimentally. Subsequently, the stability and cost of materials are further considered, further shortening the SAAs to a list of 6 binary and 142 ternary SAAs towards HERs. The experimental results also demonstrate the applicability of the CATIDPy workflow for rapidly screening superior HER electrocatalysts. Remarkably, this workflow can be easily extended to other catalytic materials and reactions.

Results and discussion

Framework of the oriented design of SAAs for HERs

To design the superior SAA catalysts for HER, the goal of the optimization problem is to locate the surface composition corresponding to the proper activity descriptor E_H (the adsorption energy of H atom; see discussions later). As shown in Fig. 1a, in the developed CATIDPy software, we adopted the genetic-algorithm-based (GA) global optimization method to determine the search direction in the structural or compositional space, which is based on evolutionary principles such as selection, crossover and mutation, and a relatively small modification or mutation of the structure could be sufficient to surpass the barrier and find a nearby local minimum. In the evolution process, each structural unit was initially encoded into a string (see Theoretical methods in the ESI†), i.e., a chromosome, and a wide variety of potential catalytic materials were subsequently generated via evolutionary operators (see Fig. 1b). Fig. 1c illustrates the whole automated and object-oriented workflow in CATIDPy for HERs on SAA catalysts, in which the on-the-fly DFT calculations can be automatically performed to investigate the activity of SAA catalysts on the basis of GA. Specifically, this process can be described as follows: (i) the unit cells of host metal can be obtained from material database according to the structural-gene-represented string, generated by GA; (ii) after relaxing the bulk unit cells of these host metals, the fcc hollow site of the (111) facet is chosen and one or two host atoms closest to the center of site are substituted by guest atoms, forming different local active-site environments (denoted as HHG_1 or HG_1G_2, where H, G_1/G_2 correspond to the host and guest atoms, respectively); (iii) the adsorption structure of atomic H is optimized on the designed active site configuration, and the DFT results are stored in a database for calculating E_H; (iv) the guest atoms are automatically selected and updated following the direction determined by GA, and this yields a closed feedback loop of high-throughput screening. Notably, the fitness function, which largely determines the convergence speed of GA towards the optimal solution, is defined as fitness$(x) = 1/|E_H(x) - E_{opt}|$ in this application for the HER, where $E_H(x)$ and E_{opt} represent the adsorption energies of atomic hydrogen (H*) of the individual (x) and target value, respectively. It is worth emphasizing that CATIDPy provides a general workflow to realize object-oriented catalyst design, which can perform on-the-fly DFT calculations for extending to other adsorbates, bulk materials, surfaces and adsorption sites with various descriptors accessible from DFT calculations.

Determination of the activity descriptor for the HER

Regarding the assignment of E_{opt}, a descriptor–activity relationship was utilized to predict the catalyst activity towards a HER prior to invoking CATIDPy, which gives an adsorption free energy of hydrogen (ΔG_H) at 0 eV (corresponding to $E_{opt} = -0.27$ eV) for the optimal activity at the working voltage of a standard hydrogen electrode.[25,30] We also considered the effect of surface coverage of the H* intermediate on the volcano-type activity trend in reality,[60–62] as shown in Fig. S1,† to obtain these potential HER catalysts more accurately. The coverage effect has little impact on the right side of the volcano curve due to the weak adsorption of the adsorbate, while a stronger adsorption of the adsorbate on the left side of volcano curve would increase the coverage, which would result in greater interactions
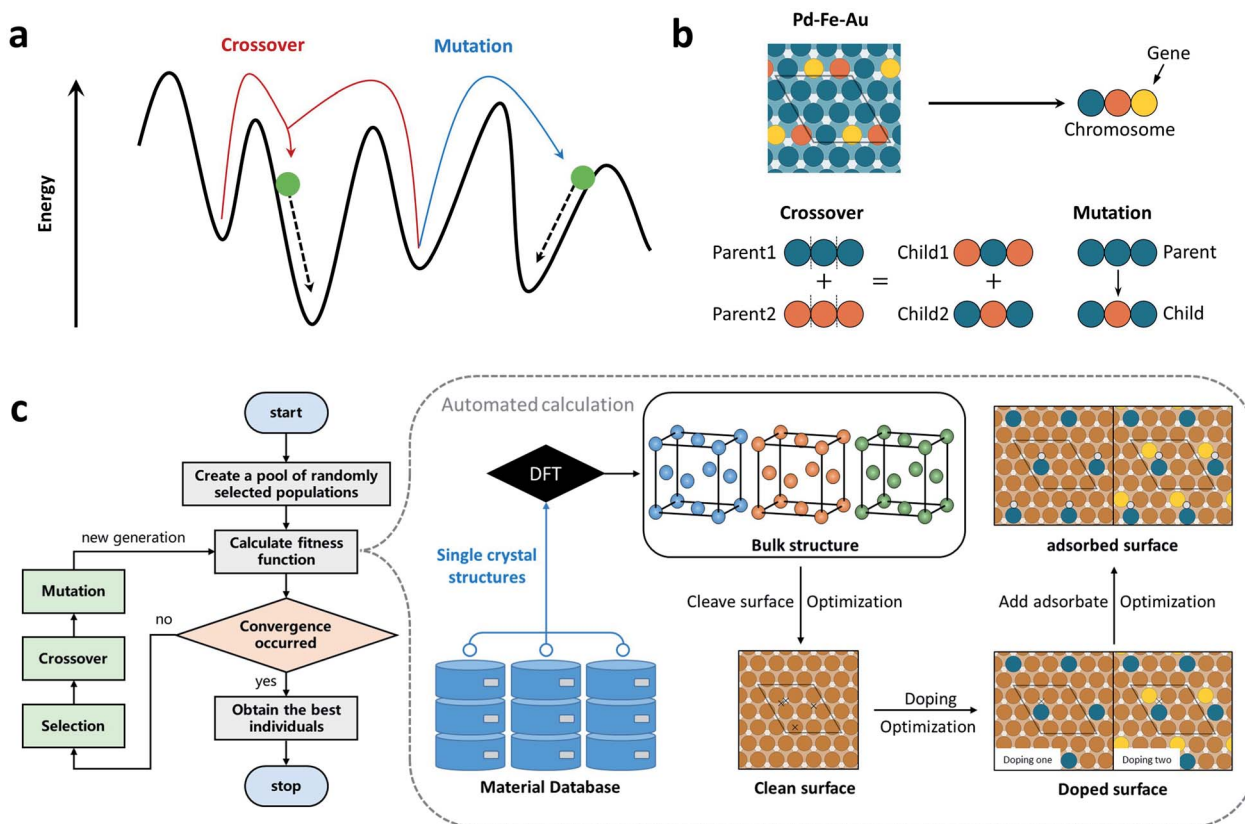
Fig. 1 (a) A diagram depicting how new structures are generated within the genetic algorithm (GA) in a potential energy surface (PES). Optimization to the nearest local minimum is represented by the bold dashed arrows. (b) A schematic illustration of how structural data are encoded into a string in the GA. Generic crossover and mutation operations are also shown. (c) CATIDPy workflow and atomic structure examples associated with each step for systematically investigating the HER activity on SAA catalysts.

between the adsorbates, thereby weakening the adsorption energy and boosting the reaction activity. Therefore, on the basis of such considerations, a range of -0.57 to -0.17 eV was utilized to discriminate the potential catalysts.

Location of active binary SAAs

Twenty-nine guest elements, of which 69% are d-block elements and 31% are p-block elements, were employed to combine with a specific host metal (*i.e.*, Cu, Ag, Au, Pt, Pd, Rh, Ir, Ni and Al) on the surface, yielding a large set of SAAs for the HERs, as shown in Fig. S2.† After one round of GA evolution to search the target combinations, which consists of 20 generations with a population size of 10 configurations for each generation, 112 binary SAAs were automatically examined by DFT calculations and stored in the search space. Fig. 2a illustrates that the E_H values of these 112 materials have a large energy range (over 3.5 eV) and uneven energy distribution. Interestingly, most of them are inside the range of $(-0.7, 0)$ eV, being around the targeted range of $(-0.57, -0.17)$ eV, which preliminarily demonstrates the efficiency of such a GA-guided search. We further explored the potential SAAs with a near-optimal E_H; it was found that there were as many as 70 candidate SAA catalysts identified by these 112 DFT calculations, which are listed in detail in Fig. 2a and Table S1.† Such a high probability (62.5%) indicates the

excellent performance of our workflow for an object-oriented catalyst design, compared to that of the pure exhaustive DFT calculations (see Fig. S3 and S4†). Remarkably, some of these 70 SAA catalysts have already been reported to be active for HERs. For example, Ni-based catalysts were shown to be active for HERs,[40–43,59] and a theoretical calculation indicated that the ΔG_H values of Pt/Au(111), Rh/Au(111) and Pt/Ag(111) are near zero, being potential HER catalysts.[63] Therefore, those that have not been tried yet are highly recommended for experimental work for HERs in the future.

The reliability of this framework is also addressed; a total of five rounds of the GA search starting from different initial conditions were independently performed, as shown in Fig. 2b. This demonstrates the high search success rate of five rounds of random tests, and especially the highly overlapped active SAA-composition space from these five parallel tests. Moreover, we retrospectively tested the iterative efficiency *via* evaluation of the best E_H at each generation. It was found that the best E_H at each generation gradually converges to the criteria (-0.27 eV). More specifically, the best E_H at each generation before the tenth generation fluctuates greatly, and then gradually converges, although there are still some small fluctuations caused by mutation. Overall, these results demonstrate the significant performance of the automation of the DFT workflow
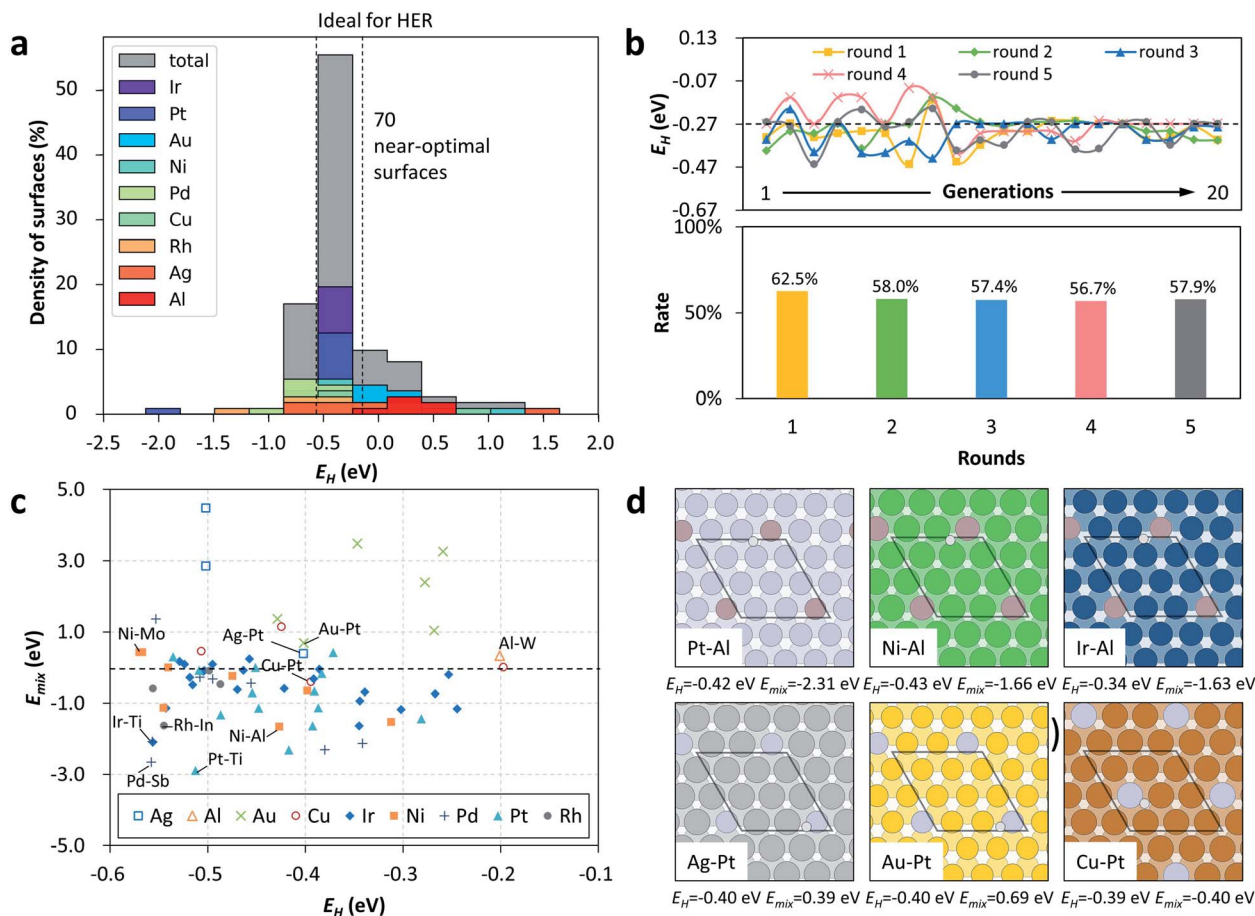
Fig. 2 (a) The distribution of hydrogen adsorption energies (E_H) on 112 binary SAAs. Each color represents an individual host metal. Note that there are 70 E_H values inside the range of −0.57 to −0.17 eV. (b) Iterative processes using the genetic algorithm show the best E_H value for each generation. The search success rate of five rounds of random tests is obtained and there are 20 generations in each round. (c) The distribution of mixing energies (E_{mix}) of 70 binary SAAs with their E_H values inside the range of −0.57 to −0.17 eV, where E_{mix} measures the thermodynamic requirements for the formation of a SAA. The same mark indicates the same host metal with a different guest metal. (d) Some potential binary SAA surface configurations are identified that justify further experimental work. Herein, the syntax for the combination of host and guest metals is H−G_1. For example, Pt−Al indicates a combination where Pt and Al are the host and guest metals, respectively.

towards an object-oriented design of active hydrogen evolution catalysts on SAAs.

To further screen out the thermodynamically easily synthesized catalytic materials in experiments from these 70 candidates, we also explored the relative stability of each SAA by evaluating the surface mixing energies (E_{mix}), which are expressed as follows:

$$E_{mix} = E(A_{n−1}B) + E_{atom}(A) − [E(A_n) + E_{atom}(B)] \quad (1)$$

$$E_{mix} = E(A_{n−2}BC) + 2E_{atom}(A) − [E(A_n) + E_{atom}(B) + E_{atom}(C)] \quad (2)$$

where $E(A_{n−1}B)$ and $E(A_{n−2}BC)$ are the total energies of surfaces of the binary and ternary SAAs, respectively, while $E_{atom}(A)$, $E_{atom}(B)$ and $E_{atom}(C)$ are the average energies of atoms A, B and C, respectively, relative to their bulk phase. The mixing energies explain the thermodynamic requirements for the formation of SAAs (see Fig. S5†); the more negative mixing energy, the less

prone to phase segregation in the SAA. Fig. 2c illustrates the distribution of E_{mix} and E_H of these 70 potential SAAs. It can be seen that there is a wide energy range of E_{mix} of about 7.40 eV. This shows, from the perspective of thermodynamics, that the synthesis of Ag- and Au-based SAA catalysts is not favored due to their relatively high E_{mix}, according with the fact that Ag and Au are generally inert in nature and do not tend to mix with other metals. In contrast, Ir, Ni, Pd, Pt and Rh as the host metals of SAAs possess a relatively low E_{mix}. Quantitatively, to allow for some leeway in the identification of promising catalytic materials, 46 binary SAAs with E_{mix} less than zero were identified (see Table S1† and Fig. 3a), which thus deserved that more attention be paid experimentally.

In addition, it is worth discussing that one can infer some basic rules on the composition pattern of these identified active and stable binary SAA candidates, which can be divided into three categories. (i) The first category is the noble host metals (Pt, Ir, Pd, Rh) that are originally active for HERs and finely modified with promising guest atoms, e.g., Pt−Al, Rh−In, Pd−Ga
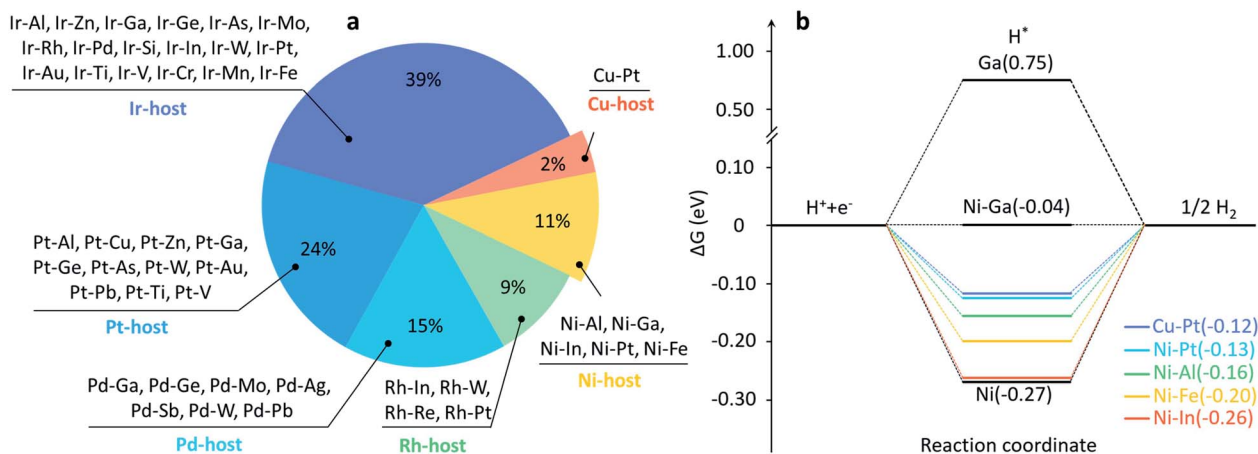
Fig. 3 (a) The identified 46 potential SAA catalysts with E_{mix} values less than zero. (b) Free energy diagrams for the hydrogen evolution reaction. Note that there are 6 potential SAA catalysts near zero, which include cost-effective Ni and Cu as host metals.

and Ir–Al, as shown in Fig. 2d and 3a. The majority of candidates are in this category, implying the more dominating role of the host metal in determining E_H. However, the expensive cost of these materials still limits their large-scale application. (ii) The second one is the inactive coinage metals (Au, Ag) as hosts doped with approximately a single guest atom, e.g., Ag–Pt, Au–Pt (see Fig. 2d). (iii) The third category is a very promising and attractive group, which comprises the cost-effective Ni and Cu as the host metals, including one Cu-based (Cu–Pt) and five Ni-based SAAs (i.e., Ni–Al, Ni–Ga, Ni–In, Ni–Pt and Ni–Fe; see Fig. 3a). Noteworthily, with the established dataset of SAA above, one can also extract some host–guest-interaction induced variation trends of E_H. Specifically, a stronger/weaker binding ability of the metal with a weaker/stronger one will produce a moderate binding ability towards the adsorption of H*. For example, ΔG_H values on pure Ga(111) and Ni(111) are 0.75 eV and −0.27 eV, respectively, while Ni–Ga SAA possesses a moderate ΔG_H of −0.04 eV (see Fig. 3b). In addition, ΔG_H values on these 6 cost-effective SAA catalysts are near zero, showing a potential activity for HERs, especially under alkaline conditions. These findings demonstrate some basic activity–composition relations in SAA-catalysis, which are conducive to the rational design or optimization of SAA-catalysts.

HER performance evaluation of the Ni-based category

To test the reliability of the CATIDPy workflow, we chose to fabricate the cost-effective Ni-based category catalysts and evaluated their HER performances. The homogeneously dispersed Ni-based binary alloys (e.g., NiMo, NiAl, Ni₃Al, NiGa and NiIn) were synthesized via a thermal hydrogen treatment method on a Ni foam substrate.[64–67] Notably, despite the fact that the prepared samples were Ni-based alloys instead of the ideal model of Ni-based single atom alloys, they featured local active sites like SAAs, with an atomically dispersed guest metal on the Ni surface layer (see details in the ESI, Fig. S8–S13†). The HER performances were evaluated in a three-electrode H-type cell with the synthesized bimetallic alloy on the Ni foam as the working electrode, an Ag/AgCl (3.5 M KCl) electrode as the

reference electrode and a graphite rod as the counter electrode, in a 1.0 M KOH alkaline electrolyte (see Experimental methods in the ESI, Fig. S14†). In Fig. 4a, the linear sweep voltammetric (LSV) curves show that all the fabricated Ni-based bimetallic electrocatalysts, which were inspired by the CATIDPy workflow, exhibit superior HER performances to that of the bare Ni foam, with obvious lower overpotentials (η) to achieve the same current densities (j). Furthermore, the corresponding η of the electrocatalysts at a j of 10, 50, 100 and 200 mA cm⁻² were also collected from at least 3 independent tests (see Fig. 4b, S15–S20 and Table S2†), which indicates the decreased η_{10}, η_{50}, η_{100} and η_{200} trend of Ni foam, NiAl, Ni₃Al, NiGa, NiIn and NiMo bimetallic electrocatalysts. It is worth mentioning that Ni₃Al displays a lower η_{10}, η_{50}, η_{100} and η_{200} at −197.22 ± 0.58, −265.69 ± 7.17, −293.98 ± 11.04 and −321.72 ± 16.82 mV than those of NiAl at −210.69 ± 5.80, −279.52 ± 4.84, −304.83 ± 5.72 and −330.61 ± 6.01 mV (Table S2†). This indicates that the Ni₃Al electrocatalyst features higher activities in both low and high overpotential regions than those of the NiAl sample, which may be attributed to more isolated Al atoms in the Ni₃Al bimetallic electrocatalyst with more SAA active sites (see Fig. S13†), and this is also consistent with the theoretical results.

Particularly, the NiMo-based bimetallic electrocatalyst exhibits the optimal alkaline HER performance among the synthesized samples, showing η_{10} and η_{200} at −52.32 ± 1.12 and −200.06 ± 6.69 mV along with Tafel slopes of 37.84 ± 3.39 and 102.05 ± 1.16 mV dec⁻¹ in the low and high overpotential regions (see Fig. 4b and S15†), respectively, which shows an excellent alkaline HER performance like those of the reported NiMo-based electrocatalysts.[64–66] Also, the superior catalytic performance of the NiMo catalyst can be seen by comparing with that of the common Pt catalyst (see Fig. S6†). Structural characterizations were further conducted to analyze this typical NiMo-based electrocatalyst. In Fig. 4c, the X-ray diffraction (XRD) analysis shows that the NiMo sample consists of crystalline NiMoO₄ and the MoNi alloy. The high angle annular dark field scanning transmission electron microscopy (HAADF-STEM) image of the NiMo sample displays a nanorod
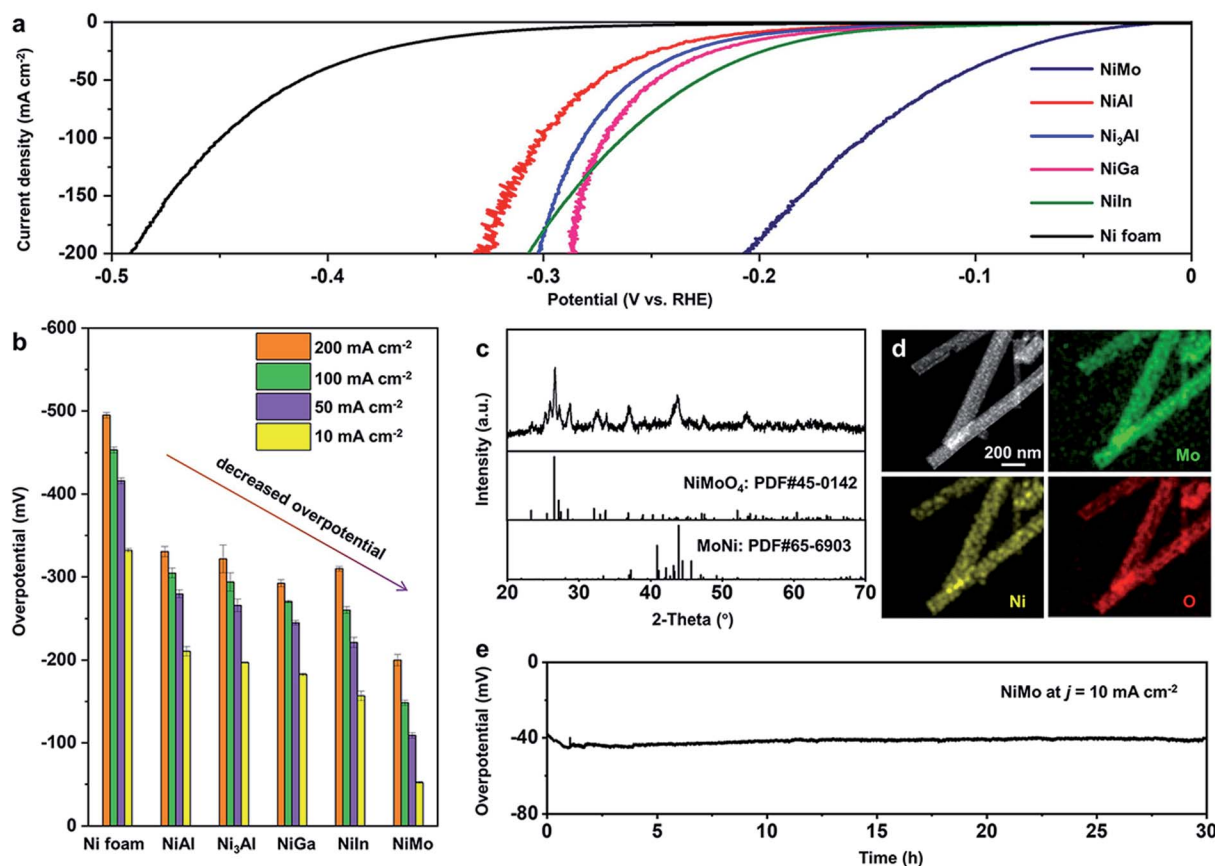
Fig. 4 (a) Typical LSV curves and (b) summarized HER performances of synthesized Ni-based bimetallic electrocatalysts with the overpotentials required to achieve 10, 50, 100, and 200 mA cm^{-2}, which were evaluated in 1.0 M KOH. All the fabricated bimetallic electrocatalysts exhibit obviously improved HER performances over that of bare Ni foam. Notes: all the bimetallic electrocatalysts were directly fabricated on a Ni foam substrate; Ni$_3$Al means a molar ratio of Ni : Al of 3 : 1 in the precursors instead of in the final sample. (c) The XRD pattern of synthesized bimetallic NiMo-based electrocatalysts, showing the sharp diffraction peaks which are assigned to the MoNi alloy and NiMoO$_4$. (d) A HAADF-STEM image of the NiMo-based electrocatalyst and corresponding mapping of Mo, Ni, and O elements, displaying the homogeneously dispersed Mo and Ni elements over the whole region and indicating the existence of the NiMo alloy. (e) The chronoamperometric curve of the NiMo-based electrocatalyst at a constant current density of 10 mA cm^{-2} for more than 30 hours without any obvious degradation, showing the robust stability in real water-splitting electrolysis testing.

morphology with a diameter of ~150 nm (see Fig. 4d). The corresponding mappings also suggest a uniform distribution of the Mo, Ni and O elements in the whole region (see Fig. 4d). The above XRD and STEM analyses unambiguously prove the existence of bimetallic NiMo alloy in the as-prepared sample. The stability of the NiMo-based electrocatalyst was examined at a constant j of 10 mA cm^{-2} with η around -40 mV, and exhibited no obvious degradation for more than 30 h of testing (see Fig. 4e), which proves its robustness in long-term electrolysis.

Taking these experimental results together, we have demonstrated the effectiveness of the CATIDPy workflow for rapidly screening efficient HER electrocatalysts. Notably, although the fabricated Ni-based bimetallic electrocatalysts do not necessarily correspond to the well-defined SAAs, the guest atoms of Al, Ga, In and Mo along with the host Ni atoms are homogeneously dispersed, decorated with active binary SAA sites in the samples. With this in mind, we anticipate well-defined SAA electrocatalysts (e.g., NiAl, NiGa, NiIn and NiMo

SAAs), which could be constructed via advanced synthesis methods, to homogeneously isolate the active SAA motifs with abundant exposed active sites to achieve extraordinary HER performances, featuring a huge potential in real-world water electrolysis techniques.

Location of more complex active ternary SAAs

Our approach has successfully achieved the screening of binary SAA catalysts, but the restriction of the binary combination resulted in only a limited number of candidate catalysts being identified on some host metals. For example, only one Cu-based binary SAA catalyst (Cu–Pt) was identified inside the range of $(-0.57, -0.17)$ eV. Thus, we further expand the material search space to ternary SAA systems to test more potential SAA catalysts on a specific host metal. Herein, we performed our workflow with ten rounds of GA to investigate ternary SAA catalysts. It is worth emphasizing that after ten rounds of GA (a total of 2000 structures generated by $10 \times 10 \times 20$), non-repetitive 1447 SAAs were explored with the DFT calculations guided by the GA, and
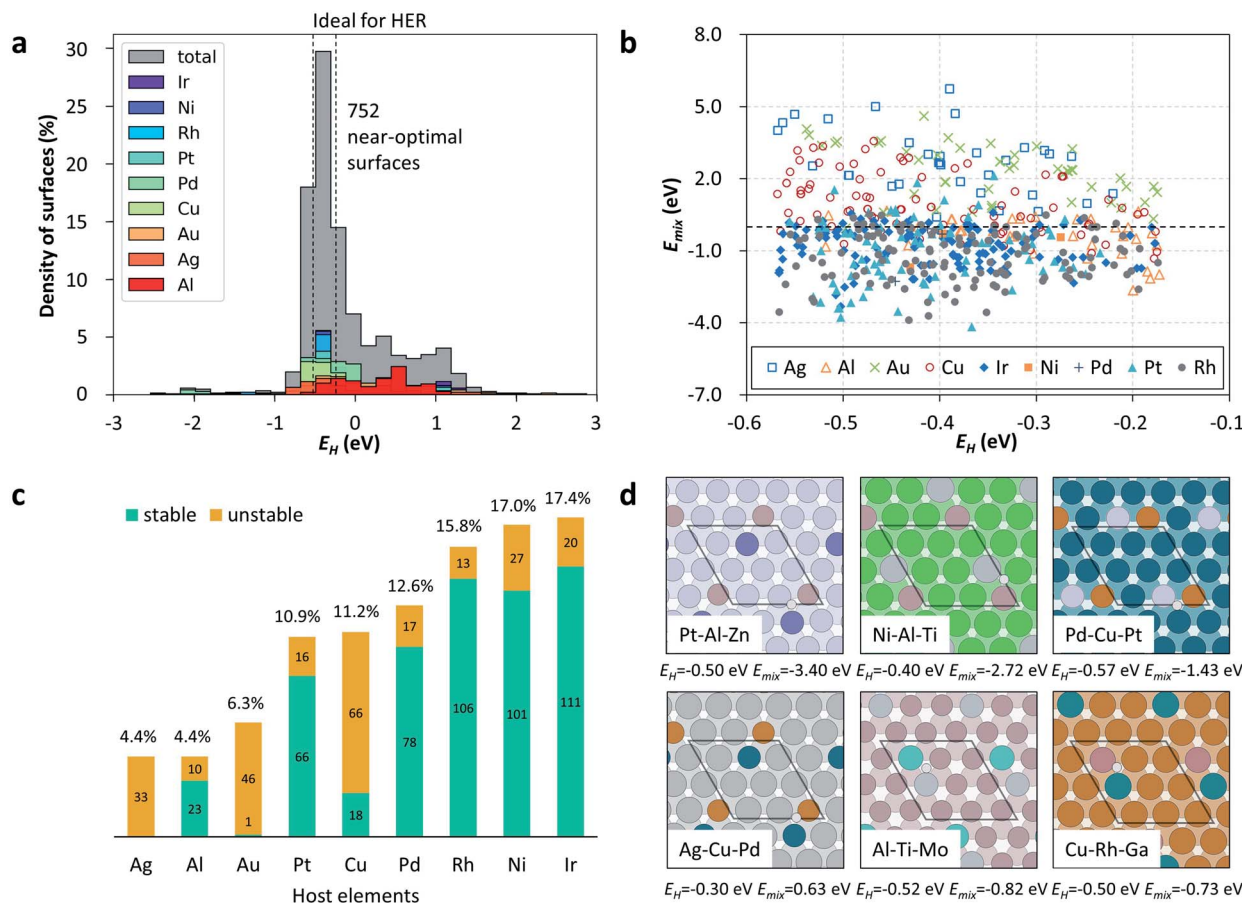
Fig. 5 (a) The distribution of E_H values of 1447 ternary SAAs. Each color represents an individual host metal. Note that there are 752 E_H values inside the range of −0.57 to −0.17 eV. (b) The distribution of the mixing energies (E_{mix}) of 752 ternary SAAs with their E_H values inside the range of −0.57 to −0.17 eV. The same mark indicates the same host metal with different guest metals. (c) The distribution of the number of potentially active SAAs on the respective host metal. (d) Some identified potential ternary SAA surface configurations that justify further experimental work. In this work, the syntax for the combination of host and guest metals is H−G_1−G_2. For example, Pt−Al−Zn indicates a combination where Pt is the host metal and Al and Zn are the guest metals.

752 near-optimal surfaces out of these 1447 SAA catalysts were identified (see Fig. 5a for details), corresponding to a success rate of 0.52, which is a more efficient way compared to the pure exhaustive method (see Fig. S4†). Likewise, we also considered E_{mix} of these 752 promising catalysts to narrow the material search space (see Table S3†). Noteworthily, ternary SAAs show more diverse combinations and a denser distribution in comparison with the binary ones, as shown in Fig. 5b. More specifically, the range of E_{mix} is from −4.17 to 5.74 eV for these 1447 SAAs and there are 504 combinations of SAAs with E_{mix} less than zero, which can be expected to be active for HERs and synthesized by experiments in the future.

Furthermore, subsequent statistical analyses also reveal the difference in the distribution of the number of SAAs in various host metals according to their E_{mix}, as illustrated by Fig. 5c. It is found that most of the Ag-, Cu- and Au-based ternary SAAs are unstable, which add up to 21.9%, and they might not be favorable to experimental synthesis due to their relatively high E_{mix}. In contrast, Pt-, Pd-, Rh-, Ni- and Ir-based ternary SAAs are the thermodynamically more stable ones, and account for

a total of 73.7%. Moreover, considering the earth-abundant and cheap Al, Ni or Cu as the host metals of SAAs, 142 ternary SAA catalysts can be further identified (see Table S3†), on which further experimental work is deserved. For example, some promising ternary SAA surface configurations, e.g., Ni–Ai–Ti, Al–Ti–Mo and Cu–Rh–Ga, are illustrated in Fig. 5d. In particular, it is worth mentioning that the Pd–Cu–Pt ternary SAA catalyst identified in this work, which possesses an E_H of −0.57 eV and E_{mix} of −1.43 eV, was explicitly verified experimentally.[57]

Conclusions

In summary, we investigated the HER on binary/ternary SAA catalysts, in which an automated and object-oriented CATIDPy workflow without user intervention and knowledge from the expert domain was proposed. This workflow achieves on-the-fly DFT calculations guided by a generic algorithm, and it is capable of screening/designing SAA catalysts for the HER, with 70 binary and 752 ternary catalyst candidates. On the basis of stability and cost, 6 cost-effective binary and 142 ternary SAA

catalysts were further identified, which are recommended for the experimental verification of their activities. In particular, based on these theoretical guidelines, homogeneously dispersed Ni-based binary SAAs were synthesized and they were verified to have superior HER performance, confirming the applicability of the CATIDPy workflow. Perhaps more importantly, such a workflow could be expandable and have significant application prospects for designing other types of catalytic materials with one or more different criteria.

Data availability

Most of the data that support the fndings of this study are present in the article and its ESI. The corresponding author will provide additional data not available in these documents upon reasonable request.

Author contributions

H. F. W. conceived the project and P. H. and J. F. C. contributed to the design of the calculations. C. Z. made the workflow, performed the calculations, and wrote the paper. P. F. L., J. Zhao, S. D., and H. G. Y. carried out the experimental work. All the authors discussed the results and commented on the manuscript. We also thank Prof. M. H. Zhu, Prof. Y. Guo, Dr X. H. Liu, and Dr L. Wang for helpful discussions relating to experimental characterization.

Conflicts of interest

There are no conflicts to declare.

Acknowledgements

Notes and references

1 F. Calle-Vallejo, O. A. Díaz-Morales, M. J. Kolb and M. T. M. Koper, *ACS Catal.*, 2015, **5**, 869–873.

2 A. J. Medford, C. Shi, M. J. Hoffmann, A. C. Lausche, S. R. Fitzgibbon, T. Bligaard and J. K. Nørskov, *Catal. Lett.*, 2015, **145**, 794–807.

3 Y. Ding, Y. Xu, Y. Mao, Z. Wang and P. Hu, *Chem. Commun.*, 2020, **56**, 3214–3217.

4 J. E. Sutton and D. G. Vlachos, *J. Catal.*, 2016, **338**, 273–283.

5 F. Abild-Pedersen, J. Greeley, F. Studt, J. Rossmeisl, T. R. Munter, P. G. Moses, E. Skúlason, T. Bligaard and J. K. Nørskov, *Phys. Rev. Lett.*, 2007, **99**, 016105.

6 A. Michaelides, Z.-P. Liu, C. Zhang, A. Alavi, D. A. King and P. Hu, *J. Am. Chem. Soc.*, 2003, **125**, 3704–3705.

7 E. M. Fernandez, P. G. Moses, A. Toftelund, H. A. Hansen, J. I. Martinez, F. Abild-Pedersen, J. Kleis, B. Hinnemann, J. Rossmeisl, T. Bligaard and J. K. Nørskov, *Angew. Chem., Int. Ed.*, 2008, **47**, 4683–4686.

8 T. Bligaard, J. K. Nørskov, S. Dahl, J. Matthiesen, C. H. Christensen and J. Sehested, *J. Catal.*, 2004, **224**, 206–217.

9 B. Meyer, B. Sawatlon, S. Heinen, O. A. von Lilienfeld and C. Corminboeuf, *Chem. Sci.*, 2018, **9**, 7069–7077.

10 A. Jain, S. P. Ong, G. Hautier, W. Chen, W. D. Richards, S. Dacek, S. Cholia, D. Gunter, D. Skinner and G. Ceder, *APL Mater.*, 2013, **1**, 011002.

11 G. Pizzi, A. Cepellotti, R. Sabatini, N. Marzari and B. Kozinsky, *Comput. Mater. Sci.*, 2016, **111**, 218–230.

12 C. Draxl and M. Scheffler, *MRS Bull.*, 2018, **43**, 676–682.

13 J. E. Saal, S. Kirklin, M. Aykol, B. Meredig and C. Wolverton, *JOM*, 2013, **65**, 1501–1509.

14 S. Curtarolo, W. Setyawan, S. Wang, J. Xue, K. Yang, R. H. Taylor, L. J. Nelson, G. L. Hart, S. Sanvito and M. Buongiorno-Nardelli, *Comput. Mater. Sci.*, 2012, **58**, 227–235.

15 D. Landis, J. Hummelshøj, S. Nestorov, J. Greeley, M. D. lak, T. Bligaard, J. Nørskov and K. Jacobsen, *Comput. Sci. Eng.*, 2012, **14**, 51–57.

16 S. Haastrup, M. Strange, M. Pandey, T. Deilmann, P. S. Schmidt, N. F. Hinsche, M. N. Gjerding, D. Torelli, P. M. Larsen and A. C. Riis-Jensen, *2D Mater.*, 2018, **5**, 042002.

17 F. H. Allen, *Acta Crystallogr., Sect. B: Struct. Sci.*, 2002, **58**, 380–388.

18 A. Belsky, M. Hellenbrandt, V. L. Karen and P. Luksch, *Acta Crystallogr., Sect. B: Struct. Sci.*, 2002, **58**, 364–369.

19 S. Gražulis, A. Daškevič, A. Merkys, D. Chateigner, L. Lutterotti, M. Quiros, N. R. Serebryanaya, P. Moeck, R. T. Downs and A. Le Bail, *Nucleic Acids Res.*, 2012, **40**, D420–D427.

20 Y. Xu, M. Yamazaki and P. Villars, *Jpn. J. Appl. Phys.*, 2011, **50**, 11RH02.

21 J. K. Nørskov and B. Hammer, *Adv. Catal.*, 2000, **31**, 71–129.

22 X. Ma and H. Xin, *Phys. Rev. Lett.*, 2017, **118**, 036101.

23 F. Calle-Vallejo, J. I. Martinez, J. M. Garcia-Lastra, P. Sautet and D. Loffreda, *Angew. Chem., Int. Ed.*, 2014, **53**, 8316–8319.

24 C. Zhou, B. Zhang, P. Hu and H. Wang, *Phys. Chem. Chem. Phys.*, 2020, **22**, 1721–1726.

25 K. Tran and Z. W. Ulissi, *Nat. Catal.*, 2018, **1**, 696–703.

26 C. Chen, W. Ye, Y. Zuo, C. Zheng and S. P. Ong, *Chem. Mater.*, 2019, **31**, 3564–3572.

27 S. Back, K. Tran and Z. W. Ulissi, *ACS Catal.*, 2019, **9**, 7651–7659.

28 J. Wang, H. Wang and P. Hu, *Sci. China: Chem.*, 2018, **61**, 336–343.

29 Z. W. Seh, J. Kibsgaard, C. F. Dickens, I. Chorkendorff, J. K. Nørskov and T. F. Jaramillo, *Science*, 2017, **355**, eaad4998.

30 J. K. Nørskov, T. Bligaard, A. Logadottir, J. Kitchin, J. G. Chen, S. Pandelov and U. Stimming, *J. Electrochem. Soc.*, 2005, **152**, J23–J26.

31 E. Skúlason, G. S. Karlberg, J. Rossmeisl, T. Bligaard, J. Greeley, H. Jónsson and J. K. Nørskov, *Phys. Chem. Chem. Phys.*, 2007, **9**, 3241–3250.

32 S. Fang, X. Zhu, X. Liu, J. Gu, W. Liu, D. Wang, W. Zhang, Y. Lin, J. Lu and S. Wei, *Nat. Commun.*, 2020, **11**, 1029–1036.

33 R. B. Wexler, J. M. P. Martirez and A. M. Rappe, *J. Am. Chem. Soc.*, 2018, **140**, 4678–4683.

34 D. D. V. Aničijević, V. M. Nikolić, M. P. Marčeta-Kaninski and I. A. Pašti, *Int. J. Hydrogen Energy*, 2013, **38**, 16071–16079.

35 Y. H. Li, J. Xing, Z. J. Chen, Z. Li, F. Tian, L. R. Zheng, H. F. Wang, P. Hu, H. J. Zhao and H. G. Yang, *Nat. Commun.*, 2013, **4**, 2500.

36 J. Xing, H. B. Jiang, J. F. Chen, Y. H. Li, L. Wu, S. Yang, L. R. Zheng, H. F. Wang, P. Hu, H. J. Zhao and H. G. Yang, *J. Mater. Chem. A*, 2013, **1**, 15258–15264.

37 J. Xing, J. F. Chen, Y. H. Li, W. T. Yuan, Y. Zhou, L. R. Zheng, H. F. Wang, P. Hu, Y. Wang, H. J. Zhao, Y. Wang and H. G. Yang, *Chem.–Eur. J.*, 2014, **20**, 2138–2144.

38 J. Kibsgaard and I. Chorkendorff, *Nat. Energy*, 2019, **4**, 430.

39 J. Wang, F. Xu, H. Jin, Y. Chen and Y. Wang, *Adv. Mater.*, 2017, **29**, 1605838.

40 I. A. Raj and K. Vasu, *J. Appl. Electrochem.*, 1990, **20**, 32–38.

41 C. Fan, D. Piron, A. Sleb and P. Paradis, *J. Electrochem. Soc.*, 1994, **141**, 382.

42 W. F. Chen, K. Sasaki, C. Ma, A. I. Frenkel, N. Marinkovic, J. T. Muckerman, Y. Zhu and R. R. Adzic, *Angew. Chem., Int. Ed.*, 2012, **51**, 6131–6135.

43 Q. Zhang, P. Li, D. Zhou, Z. Chang, Y. Kuang and X. Sun, *Small*, 2017, **13**, 1701648.

44 R. T. Hannagan, D. A. Patel, L. A. Cramer, A. C. Schilling, P. T. Ryan, A. M. Larson, V. Çınar, Y. Wang, T. A. Balema and E. C. H. Sykes, *ChemCatChem*, 2020, **12**, 488–493.

45 M. T. Darby, R. Réocreux, E. C. H. Sykes, A. Michaelides and M. Stamatakis, *ACS Catal.*, 2018, **8**, 5038–5050.

46 M. D. Marcinkowski, M. T. Darby, J. Liu, J. M. Wimble, F. R. Lucci, S. Lee, A. Michaelides, M. Flytzani-Stephanopoulos, M. Stamatakis and E. C. H. Sykes, *Nat. Chem.*, 2018, **10**, 325.

47 M. T. Greiner, T. Jones, S. Beeg, L. Zwiener, M. Scherzer, F. Girgsdies, S. Piccinin, M. Armbrüster, A. Knop-Gericke and R. Schlögl, *Nat. Chem.*, 2018, **10**, 1008–1015.

48 G. Kyriakou, M. B. Boucher, A. D. Jewell, E. A. Lewis, T. J. Lawton, A. E. Baber, H. L. Tierney, M. Flytzani-Stephanopoulos and E. C. H. Sykes, *Science*, 2012, **335**, 1209–1212.

49 M. T. Darby, M. Stamatakis, A. Michaelides and E. C. H. Sykes, *J. Phys. Chem. Lett.*, 2018, **9**, 5636–5646.

50 G. Sun, Z.-J. Zhao, R. Mu, S. Zha, L. Li, S. Chen, K. Zang, J. Luo, Z. Li and S. C. Purdy, *Nat. Commun.*, 2018, **9**, 4454–4462.

51 F. Xing, J. Jeon, T. Toyao, K.-i. Shimizu and S. Furukawa, *Chem. Sci.*, 2019, **10**, 8292–8298.

52 P. Aich, H. Wei, B. Basan, A. J. Kropf, N. M. Schweitzer, C. L. Marshall, J. T. Miller and R. Meyer, *J. Phys. Chem. C*, 2015, **119**, 18140–18148.

53 J. Shan, J. Liu, M. Li, S. Lustig, S. Lee and M. Flytzani-Stephanopoulos, *Appl. Catal., B*, 2018, **226**, 534–543.

54 G. Rupprechter, *Nat. Chem.*, 2017, **9**, 833–834.

55 F. R. Lucci, J. Liu, M. D. Marcinkowski, M. Yang, L. F. Allard, M. Flytzani-Stephanopoulos and E. C. H. Sykes, *Nat. Commun.*, 2015, **6**, 8550–8557.

56 J. Liu, F. R. Lucci, M. Yang, S. Lee, M. D. Marcinkowski, A. J. Therrien, C. T. Williams, E. C. H. Sykes and M. Flytzani-Stephanopoulos, *J. Am. Chem. Soc.*, 2016, **138**, 6396–6399.

57 T. Chao, X. Luo, W. Chen, B. Jiang, J. Ge, Y. Lin, G. Wu, X. Wang, Y. Hu, Z. Zhuang, Y. Wu, X. Hong and Y. Li, *Angew. Chem., Int. Ed.*, 2017, **56**, 16047–16051.

58 C. H. Chen, D. Wu, Z. Li, R. Zhang, C. G. Kuai, X. R. Zhao, C. K. Dong, S. Z. Qiao, H. Liu and X. W. Du, *Adv. Energy Mater.*, 2019, **9**, 1803913.

59 M. Li, K. Duanmu, C. Wan, T. Cheng, L. Zhang, S. Dai, W. Chen, Z. Zhao, P. Li, H. Fei, Y. Zhu, R. Yu, J. Luo, K. Zang, Z. Lin, M. Ding, J. Huang, H. Sun, J. Guo, X. Pan, W. Goddard III, P. Sautet, Y. Huang and X. Duan, *Nat. Catal.*, 2019, **2**, 495–503.

60 L. C. Grabow, B. Hvolbæk and J. K. Nørskov, *Top. Catal.*, 2010, **53**, 298–310.

61 L. Qi and J. Li, *J. Catal.*, 2012, **295**, 59–69.

62 A. C. Lausche, A. J. Medford, T. S. Khan, Y. Xu, T. Bligaard, F. Abild-Pedersen, J. K. Nørskov and F. Studt, *J. Catal.*, 2013, **307**, 275–282.

63 M.-J. Cheng, E. L. Clark, H. H. Pham, A. T. Bell and M. Head-Gordon, *ACS Catal.*, 2016, **6**, 7769–7777.

64 Y. Y. Chen, Y. Zhang, X. Zhang, T. Tang, H. Luo, S. Niu, Z. H. Dai, L. J. Wan and J. S. Hu, *Adv. Mater.*, 2017, **29**, 1703311.

65 J. Zhang, T. Wang, P. Liu, Z. Liao, S. Liu, X. Zhuang, M. Chen, E. Zschech and X. Feng, *Nat. Commun.*, 2017, **8**, 15437–15444.

66 W. Du, Y. Shi, W. Zhou, Y. Yu and B. Zhang, *Angew. Chem., Int. Ed.*, 2021, **60**(13), 7051–7055.

67 G. Meng, J. Sun, L. Tao, K. Ji, P. Wang, Y. Wang, X. Sun, T. Cui, S. Du, J. Chen, D. Wang and Y. Li, *ACS Catal.*, 2021, **11**, 1886–1896.